

# Metallic and semi-conducting resistivity behaviour of $\text{La}_{0.7}\text{Ca}_{0.3-x}\text{K}_x\text{MnO}_3$ ( $x = 0.05, 0.1$ ) manganites

Dinesh Varshney · Neha Dodiya

Received: 30 September 2014 / Accepted: 23 November 2014 / Published online: 13 December 2014  
© The Author(s) 2014. This article is published with open access at Springerlink.com

**Abstract** The temperature dependence of electrical resistivity,  $\rho$ , of ceramic  $\text{La}_{0.7}\text{Ca}_{0.3-x}\text{K}_x\text{MnO}_3$  ( $x = 0.05, 0.1$ ) is investigated in metallic and semi-conducting phase. The metallic resistivity is attributed to be caused by electron–phonon, electron–electron and electron–magnon scattering. Substitutions affect average mass and ionic radii of A–site resulting in an increase in Debye temperature  $\theta_D$  attributed to hardening of lattice with K doping. The optical phonon modes shift gradually to lower mode frequencies leading to phonon softening. Estimated resistivity compared with reported metallic resistivity, accordingly  $\rho_{\text{diff.}} = [\rho_{\text{exp.}} - \{\rho_0 + \rho_{\text{e-ph}} (= \rho_{\text{ac}} + \rho_{\text{op}})\}]$ , infers electron–electron and electron–magnon dependence over most of the temperature range. Semi-conducting nature is discussed with variable range hopping and small polaron conduction model. The decrease in activation energies and increase in density of states at the Fermi level with enhanced Ca doping is consistently explained by cationic disorder and Mn valence.

**Keywords** Magnetic materials · Ab initio calculations · Electrical properties · Phonons

## Introduction

The unique properties of mixed-valence manganites as  $\text{La}_{1-x}\text{A}_x\text{MnO}_3$  ( $A = \text{Na}, \text{K}, \text{Rb}$ ) depend mainly on the relative amount of  $\text{Mn}^{3+}$  and  $\text{Mn}^{4+}$  ions. Of particular

interest are the monovalent-doped manganites as the substitution with alkali metal ions can induce twice the increase in  $\text{Mn}^{4+}$  ions as compared to the alkaline-earth metal substitution. Most of the literature is devoted to the interplay between magnetic and transport properties [1, 2]. While discussing the correlation between the magnetic and transport properties, ideas such as double-exchange (DE) mechanism and the Jahn–Teller (JT) formation have been proposed. The metallic behaviour is usually described in terms of electron–phonon interaction, and polaronic conduction mechanism is effective in describing semiconducting behaviour above  $T_C$  [3].

Raman, infrared spectroscopy and neutron inelastic scattering measurements had obtained the most convincing evidence for the phonons and structural properties related to phase transition. Raman spectroscopy measurement of  $\text{La}_{0.7}\text{Ca}_{0.3-x}\text{K}_x\text{MnO}_3$  ( $x = 0.05, 0.1$ ) confirmed the structural lattice disorder with orthorhombic to rhombohedral structure and identified three peaks. The spectral maxima of the above are mainly located in the three intervals at about 150–200, 600–700 and 1,050–1,100  $\text{cm}^{-1}$ , respectively [4].

The  $\text{La}_{0.7}\text{Ca}_{0.3-x}\text{K}_x\text{MnO}_3$  manganites show an orthorhombic structure with space group  $Pnma$  for ( $x = 0.05$ ) and rhombohedral structure with space group  $R\bar{3}C$  for ( $x = 0.1$ ) and illustrate a metallic behaviour below a temperature referred as metal–insulator transition temperature ( $T_{MI}$ ) and behave like a semiconductor above that temperature. For  $\text{La}_{0.7}\text{Ca}_{0.3-x}\text{K}_x\text{MnO}_3$ ,  $T_{MI}$  enhances with the increased K doping concentration and is 269 (275) K for  $x = 0.05$  (0.1) [5].

The disordered Holstein double-exchange model is solved to investigate the disorder effect at strong electron–phonon coupling and notice that even weak disorder enormously enhances the resistivity  $\rho$  at  $T = 0$  K,

D. Varshney (✉) · N. Dodiya  
Materials Science Laboratory, School of Physics,  
Vigyan Bhawan, Devi Ahilya University,  
Khandwa Road Campus, Indore 452001, India  
e-mail: vdinesh33@rediffmail.com

simultaneously suppressing the density of states at the Fermi level [6]. The conductivity behaviour of doped manganites in the low-temperature ferromagnetic regime ( $T < T_{MI}$ ) documents metallic behaviour, and the data have been fitted with different theoretical expressions to find the best fit. No systematic effort has been made to understand the electrical resistivity in the ferromagnetic metallic and paramagnetic semi-conducting phase of monovalent-doped manganites as  $\text{La}_{0.7}\text{Ca}_{0.3-x}\text{K}_x\text{MnO}_3$ .

The electrical resistivity of the pristine  $\text{Pr}_{2/3}(\text{Ba}_{1-x}\text{Cs}_x)_{1/3}\text{MnO}_3$  (PBMO) documents two metal–insulator transitions which are systematically shifted to lower temperatures with Cs doping. An upturn in resistivity behaviour below 50 K in PBMO manganites were explained due to the combined effect of weak localization, electron–electron and electron–phonon scattering [7]. An analogous analysis at low temperature well below  $T_{MI}$  was also put forward in the  $\text{La}_{2/3}\text{Ca}_{1/3}\text{MnO}_3$  manganites [8].

Rozenberg [9] commented on resistivity fitting of manganites at low temperature by Chen et al. [8] as the claim seems to be doubtful due to the fundamental inapplicability of the existence of low temperature minimum resulting from the existence of the intrinsic spin disorder. It stressed that the spin-dependent tunnelling and scattering of carriers between grains (grain-boundary effect) account reasonably for the resistivity minima [9]. The ferromagnetic transition in  $\text{La}_{0.75}\text{Ca}_{0.25}\text{MnO}_3$  manganites is driven by an exchange interaction of polaronic carriers with localized spins [10]. An additional contribution arising from the electron–electron contribution in  $\text{La}_{0.91}\text{Rb}_{0.06}\text{Mn}_{0.94}\text{O}_3$  must analyse the ferromagnetic metallic resistivity behaviour [11–13].

In the high-temperature semi-conducting regime ( $T > T_{MI}$ ), the electrical conduction is explained either by the spin polaronic conduction (SPC) model [14] or by the Mott’s variable range hopping (VRH) model [15]. The doping at main site influences the polaronic transport as it causes change in the Polaron hopping distance and also the polaron concentration [16]. For  $T > T_{MI}$ , the resistivity data of the Co-doped bilayer manganites  $\text{LaSr}_2\text{Mn}_2\text{O}_7$  could be fit well using the VRH model and the SPC model and also using thermally activated conduction (TAC) law [17].

Looking to earlier experimental and theoretical effort neither temperature-independent (<20 K) nor temperature-dependent (>50 K) resistivity in divalent alkaline-earth metals (Ca, Sr, and Ba) or monovalent alkali metals like Na, K, Rb, there is a clear need to properly understand the resistivity behaviour. It is worth commenting that for doped monovalent alkali metals like K at Ca site in  $\text{La}_{0.7}\text{Ca}_{0.3-x}\text{K}_x\text{MnO}_3$ , no theoretical efforts have been made so far. In view of the electron–electron ( $T^2$ ) and electron–magnon ( $T^{4.5}$ ) contributions apart from electron–phonon scattering

to resistivity, the time-tested strategy is to seek their roles in  $\text{La}_{0.7}\text{Ca}_{0.3-x}\text{K}_x\text{MnO}_3$  manganites.

We first discuss the interaction potential, which includes the long-range Coulomb interaction, van der Waals (vdW) interaction and the short-range repulsive interaction up to second-neighbour ions [18–24]. It makes us to compute the Debye and Einstein temperatures of  $\text{La}_{0.7}\text{Ca}_{0.3-x}\text{K}_x\text{MnO}_3$ . Later on, we shall use the Bloch–Gruneisen method to estimate the independent contributions of acoustic and optical phonons and both. We further compute resistivity behaviour for semi-conducting region, with both Mott’s variable range hopping (VRH) model and small polaron conduction (SPC). The technical details of the numerical analysis and its results are discussed in Sect. 3.

The main findings for resistivity behaviour in  $\text{La}_{0.7}\text{Ca}_{0.3-x}\text{K}_x\text{MnO}_3$  [ $x = 0.05$  (0.1)] include the following:

- (i) The estimated Debye and Einstein temperatures from the EIoIP are consistent with the specific heat measurements and Raman spectroscopy results.
- (ii) The Debye temperatures increase with enhanced K doping concentration results in lattice hardening.
- (iii) The optical phonon modes shift gradually to lower mode frequencies with increased doping concentration.
- (iv) The classical electron–phonon model of resistivity, for example., the Bloch–Gruneisen (BG) model retraces the reported metallic resistivity behaviour in the temperature range [ $T < T_{MI} \cong 269$  (275) K].
- (v) The quadratic temperature ( $T^2$ ) dependence of  $\rho_{\text{diff}}$ . [ $=\rho_{\text{exp.}}-(\rho_0 + \rho_{\text{e-ph}})$ ] is interpreted in terms of 3D electron–electron inelastic scattering and is essential for the description of resistivity.
- (vi) The  $T^{4.5}$  temperature dependence of  $\rho_{\text{diff}}$ . [ $=\rho_{\text{exp.}}-(\rho_0 + \rho_{\text{e-ph}} + \rho_{\text{e-e}})$ ] accounting for electron–magnon interactions is also essential for the correct description of resistivity.
- (vii) The  $\text{La}_{0.7}\text{Ca}_{0.3-x}\text{K}_x\text{MnO}_3$  [ $x = 0.05$  (0.1)] is a good metal in the temperature region  $T < T_{MI}$  and Mott–Ioffe–Regel criterion for metallic conductivity is valid,  $k_F l > 1$ ,  $\varepsilon_F \tau > 1$ .
- (viii) The VRH model is inappropriate for the description of resistivity behaviour in the high-temperature region,  $T > T_{MI}$ .
- (ix) The small Polaron conduction model consistently explains the higher temperature resistivity behaviour ( $T > \theta_D/2$ ).

To our knowledge, the importance of electron–phonon, electron–electron and electron–magnon interactions and small polaron conduction for the metallic and semi-conducting resistivity behaviour of  $\text{La}_{0.7}\text{Ca}_{0.3-x}\text{K}_x\text{MnO}_3$  [ $x = 0.05$  (0.1)] manganites are analysed for the first time. We end up with a summary and conclusions in Sect. 4.

### The model

The Raman spectroscopy is an impressive technique that probes the lattice vibrational properties, which not only identifies the spin–phonon interaction but also accounts for the electron–phonon interaction and is effective in mixed-valent manganites. The ideal perovskite  $ABO_3$  of cubic structure presents around 15 normal modes of vibration. The lowest frequency (external mode) corresponds to a vibration of the  $A$  ions against the rigid  $BO_6$  octahedra. The intermediate frequency (bending mode) corresponds to a vibration where the  $B$  ion and two apical oxygen molecules move against the other four oxygen molecules of the octahedron. At the highest frequency (stretching mode), the  $B$  ion moves against the rigid oxygen octahedron [25]. We can thus model the phonon spectrum consisting of an acoustic branch of Debye type and a separated optical peak with the characteristic Einstein temperature.

The dynamic properties of materials are inhibited in an effective interionic potential. This is particularly important in  $La_{0.7}Ca_{0.3-x}K_xMnO_3$ , as there is much disagreement as to whether long- or short-range interactions are at the origin. For simplification, we assume that the change in force constants is small, the short-range interactions are effective up to the second-neighbour ions and harmonic elastic forces hold the atoms together without any internal strains within the crystal. We thus express the crystal energy for a particular lattice separation ( $r$ ) as

$$U(r) = U_C(r) + U_R(r) + U_V(r). \tag{1}$$

The Coulomb energy is the first term:

$$U_C(r) = - \sum_{ij} \frac{Z_i Z_j e^2}{r_{ij}} = - \frac{\alpha_m Z^2 e^2}{r}. \tag{2}$$

$\alpha_m$  is the Madelung constant [18] and  $r_{ij}$  being the separation distance between  $i$  and  $j$  ions.

The second term in Eq. (1) refers to the short-range overlap repulsive energy and is

$$U_R(r) = nb\beta_{ij} \exp\left(\frac{r_i + r_j - r_{ij}}{\rho}\right) + n'b\beta_{ii} \exp\left(\frac{2r_i - kr_{ij}}{\rho}\right) + n'b\beta_{jj} \exp\left(\frac{2r_j - kr_{ij}}{\rho}\right). \tag{3}$$

The short-range overlap repulsive energy is written as suggested by Hafemeister and Flygare approach [18–24]. The ionic radii are  $r_i$  and  $r_j$ ,  $k$  is the structure factor, and  $n(n')$  is the number of nearest (next nearest) ions, respectively. Further, the notations  $b$  and  $\rho$  denote the hardness and range parameters, respectively.

The Pauling coefficients,  $\beta_{ij}$ , are defined in terms of valence [ $Z_i$  ( $Z_j$ )] and the number of outermost electrons [ $n_i$  ( $n_j$ )] in the anions (cations), respectively, as

$$\beta_{ij} = 1 + (Z_i/n_i) + (Z_j/n_j). \tag{4}$$

The last term in Eq. (1) is the van der Waals (vdW) energy and is

$$U_V(r) = - \left( \sum_{ij} \frac{c_{ij}}{r_{ij}^6} + \sum_{ij} \frac{d_{ij}}{r_{ij}^8} \right) \tag{5}$$

$$= - \left( \frac{C}{r^6} + \frac{D}{r^8} \right). \tag{6}$$

The van der Waals (vdW) energy is attributed to dipole–dipole ( $d$ – $d$ ) and dipole–quadruple ( $d$ – $q$ ) interactions. The overall vdW coefficients  $C$  and  $D$  in Eq. (1) are defined as [26]

$$C = c_{ij}S_6(r) + \frac{1}{2}(c_{ii} + c_{jj})S_6(0) \tag{7}$$

and

$$D = d_{ij}S_8(r) + \frac{1}{2}(d_{ii} + d_{jj})S_8(0). \tag{8}$$

$c_{ij}$  and  $d_{ij}$  are the vdW coefficients due to  $d$ – $d$  and  $d$ – $q$  interactions. We follow the variational method [27] to derive as

$$c_{ij} = \frac{3}{2} \frac{e\hbar}{\sqrt{m_e}} \alpha_i \alpha_j \left[ (\alpha_i/N_i)^{1/2} + (\alpha_j/N_j)^{1/2} \right]^{-1} \tag{9}$$

and

$$d_{ij} = \frac{27\hbar^2}{8m} \alpha_i \alpha_j \left[ (\alpha_i/N_i)^{1/2} + (\alpha_j/N_j)^{1/2} \right]^2 \left[ (\alpha_i/N_i) + \frac{20}{3} (\alpha_i \alpha_j / N_i N_j)^{1/2} + (\alpha_j/N_j) \right]^{-1}. \tag{10}$$

Here,  $m_e$  is the electron mass,  $\alpha_I$  is the electronic polarizability and  $N_i$  denotes the effective number of electrons of the  $i$ th ion. The values of the overall vdW coefficients are obtained using Eqs. (7) and (8) and weighted in terms of appropriate lattice sums [ $S_6(0)$ ,  $S_6(r)$ ,  $S_8(0)$  and  $S_8(r)$ ] [26]. The individual vdW coefficients  $c_{ij}$  and  $d_{ij}$  are obtained with certainty and accuracy as the excitation energies are ignored in Eqs. (9) and (10).

We shall seek the interionic interaction in between a pair such as Mn–O and La/Ca/K–O. It is clear from the above descriptions that the present effective interionic potential contains only two free parameters ( $b$  and  $\rho$ ), which are determined from the equilibrium conditions:

$$\left( \frac{dU}{dr} \right)_{r=r_0} = 0 \tag{11}$$

and bulk modulus

$$B_T = \frac{1}{9kr_0} \left( \frac{d^2U}{dr^2} \right)_{r=r_0}. \tag{12}$$

The model parameters obtained from Eq's. (11) and (12) have been used to compute the second-order elastic constants ( $C_{11}$ ,  $C_{12}$  and  $C_{44}$ ) as [28–31]

$$C_{11} = \frac{e^2}{4r_0^4} \left[ -5.112Z_m^2 + A_1 + \frac{(A_2 + B_2)}{2} \right], \quad (13)$$

$$C_{12} = \frac{e^2}{4r_0^4} \left[ 0.226Z_m^2 - B_1 + \frac{(A_2 - 5B_2)}{2} \right], \quad (14)$$

$$C_{44} = \frac{e^2}{4r_0^4} \left[ 2.556Z_m^2 + B_1 + \frac{(A_2 + 3B_2)}{4} \right]. \quad (15)$$

The short-range parameters for the nearest and the next nearest neighbours are ( $A_1$ ,  $B_1$ ) and ( $A_2$ ,  $B_2$ ), respectively. These are defined as

$$A_1 = \frac{4r_0^3}{e^2} \left[ \frac{d^2}{dr^2} V_{ij}(r) \right]_{r=r_0}, \quad (16)$$

$$A_2 = \frac{4(r_0\sqrt{2})^3}{e^2} \left[ \frac{d^2}{dr^2} V_{ii}(r) + \frac{d^2}{dr^2} V_{jj}(r) \right]_{r=r_0\sqrt{2}}, \quad (17)$$

$$B_1 = \frac{4r_0^3}{e^2} \left[ \frac{d}{dr} V_{ij}(r) \right]_{r=r_0}, \quad (18)$$

$$B_2 = \frac{4(r_0\sqrt{2})^2}{e^2} \left[ \frac{d}{dr} V_{ii}(r) + \frac{d}{dr} V_{jj}(r) \right]_{r=r_0\sqrt{2}}. \quad (19)$$

The short-range potentials between the ions is  $V_{ij}(r)$  and is written as

$$V_{ij}(r) = b\beta_{ij} \exp\left(\frac{r_i + r_j - r_{ij}}{\rho}\right) + c_{ij}r_{ij}^{-6} + d_{ij}r_{ij}^{-8}. \quad (20)$$

The elastic force constant  $\kappa$  is derived at the equilibrium inter-ionic distance  $r_0$  as

$$\kappa = \frac{r_0}{2} [\pi^2(C_{11} - C_{12})(C_{11} + C_{12} + 2C_{44})(C_{44})]^{1/3}. \quad (21)$$

We have thus computed the elastic force constants for a pair such as Mn–O and La/Ca/K–O and have the total elastic force constants of the K-doped  $\text{La}_{0.7}\text{Ca}_{0.3}\text{MnO}_3$ . This continuum model thus takes care of the clear physical binding in doped manganites. We stress that simpler models based on this potential can describe those cohesive properties of such solids that depend on van der Waals interactions. However, the true potential must recognize the correct charge distribution and the relative orientations of the interacting atoms in manganites, which is a complicated task.

We shall now estimate the acoustic Debye branch characterized by the Debye temperature  $\theta_D$  and an optical peak defined by the Einstein temperature  $\theta_E$ . The Debye frequency is characterized as a cutoff frequency at the Brillouin zone boundary. It can be expressed in terms of the effective value of ionic mass and elastic force constant for crystal

lattices with two different kinds of atoms such as Mn–O and La/Ca/K–O, which we deal with. The acoustic-mode and optical-mode frequencies are estimated in an ionic model using a value of effective ion charge  $Ze = -2e$ .

For the sake of simplicity, we have chosen an acoustic mass  $M = (2M_+ + M_-)$  [Mn(O) which is symbolized by  $M_+$  ( $M_-$ )];  $\kappa^* = 2\kappa$  for each directional oscillation mode to get the acoustic phonon frequency as [32–37]

$$\omega_D = \sqrt{\frac{2\kappa^*}{M}}. \quad (22)$$

In this regard, for a pairwise potential, the photons are optic in origin and the frequency is determined by the reduced mass of the pair as  $\mu^{-1} = M(A)^{-1} + M(B)^{-1}$ , where  $A$  is the cation (La/Ca/K, Mn) and  $B$  is the anion (O)

$$\omega_{LO}^2 = \frac{\kappa + \alpha}{\mu}, \quad (23)$$

$$\omega_{TO}^2 = \frac{\kappa - \alpha}{\mu}. \quad (24)$$

Here,  $\alpha$  is the force constant as

$$\alpha = \frac{8\pi(Ze)^2}{3\Omega}, \quad (25)$$

$\omega_{LO}$  ( $\omega_{TO}$ ) symbolized for the longitudinal (transverse) optical phonon frequency and  $\Omega$  for the volume of the unit cell.

It is known to us that in the metallic state, the electron–phonon, electron–electron, electron–magnon scattering and polaronic effects are the major proponents of various conceptions in electrical transport. We shall begin with the description of the scattering of electron–phonon for the resistivity in the ferromagnetic metallic state. The temperature-dependent part of the metallic resistivity, following the Debye model, is

$$\rho \approx \left(\frac{3}{\hbar e^2 v_F^2}\right) \frac{k_B T}{M v_s^2} \int_0^{2k_F} |F(q)|^2 \left[ \frac{xq^3 dq}{[e^x - 1][1 - e^{-x}]} \right], \quad (26)$$

with  $x = \hbar\omega/k_B T$ . In the above equation,  $F(q)$  is the Fourier transform of the potential associated with one lattice site,  $v_F$  being the Fermi velocity and  $v_s$  being the sound velocity. Equation (26) shows in terms of acoustic phonon contribution yields the Bloch–Grüneisen function of temperature dependence of resistivity:

$$\rho_{ac}(T, \theta_D) = 4A_{ac} T (T/\theta_D)^4 \int_0^{\theta_D/T} x^5 (e^x - 1)^{-1} (1 - e^{-x})^{-1} dx, \quad (27)$$

where  $A_{ac}$  is a constant of proportionality defined as

$$A_{ac} \cong \frac{3\pi^2 e^2 k_B}{k_F^2 v_s^2 L \hbar v_F^2 M}. \quad (28)$$

Since the resistivity is additive, the Matthiessen rule is obeyed, and resistivity is represented as a sum  $\rho(T) = \rho_0 + \rho_{e-ph}(T)$ , where  $\rho_0$  is the residual resistivity that does not depend on temperature as electrons also scatter off impurities, defects and disordered regions. However, in case of the Einstein type of phonon spectrum, (an optical mode)  $\rho_{op}(T)$  may be described as follows:

$$\rho_{op}(T, \theta_E) = A_{op} \theta_E^2 T^{-1} [e^{\theta_E/T} - 1]^{-1} [1 - e^{-\theta_E/T}]^{-1}, \quad (29)$$

$A_{op}$  is defined analogously to Eq. (28).

We have thus conveniently modelled the phonon resistivity in the ferromagnetic metallic state by combining both terms arising from acoustic and optical phonons

$$\rho_{e-ph}(T) = \rho_{ac}(T, \theta_D) + \rho_{op}(T, \theta_E). \quad (30)$$

The total resistivity is given by

$$\begin{aligned} \rho(T, \theta_D, \theta_E) &= \rho_0 + \rho_{ac}(T, \theta_D) + \rho_{op}(T, \theta_E) \\ &= \rho_0 + 4A_{ac}(T/\theta_D)^4 T \\ &\quad \times \int_0^{\theta_D/T} x^5 (e^x - 1)^{-1} (1 - e^{-x})^{-1} dx \\ &\quad + A_{op} \theta_E^2 T^{-1} [\exp(\theta_E/T) - 1]^{-1} [1 - \exp(-\theta_E/T)]^{-1}. \end{aligned} \quad (31)$$

In order to analyse the resistivity data of high-temperature region,  $T > T_{MI}$ , we have made computation following Model I: variable range hopping (VRH) and Model II: adiabatic small Polaron Conduction (SPC). In the high-temperature range, for example, in the paramagnetic semi-conducting state, we have fitted the resistivity data using VRH model.

The expression as derived by Mott for conductivity is as follows:

$$\sigma = \sigma_{oh} \exp(-T_0/T)^{0.25}. \quad (32)$$

with  $\sigma_{oh}$  as a constant and  $T_0$  defined in terms of the density of state in the vicinity of Fermi energy  $N(\epsilon_F)$  and the localization length  $a$  as

$$T_0 = \frac{18}{k_B N(\epsilon_F) a^3}. \quad (33)$$

Here  $T_o$  describes hopping transport in doped manganites where the carriers are localized by random potential fluctuations and preferred hopping is between sites lying within a certain range of energy.

Let us now briefly sketch the description of resistivity in the temperature range  $T > T_{MI}$ , associated with Model II. It is worth mentioning that the most rapid motion of a small polaron occurs when the carrier hops each time the configuration of vibrating atoms in an adjacent site coincides

with that in the occupied site. Henceforth, the charge carrier motion within the adiabatic regime is faster than the lattice vibrations, and the resistivity for SPC is as follows:

$$\rho = \rho_{os} T \exp\left(\frac{E_p}{k_B T}\right), \quad (34)$$

where  $E_p$  is the polaron formation energy and  $k_B$  being the Boltzmann constant. The resistivity coefficient  $\rho_{os}$  is given by

$$\rho_{os} = \frac{k_B}{n(1-x)e^2 D}. \quad (35)$$

Here,  $n$  is charge carrier density ( $\sim 10^{20} \text{ cm}^{-3}$ ),  $x$  is the hole ( $\text{Mn}^{4+}$ ) content,  $e$ , the electronic charge and  $D$  is the polaron diffusion constant. The polaron diffusion constant for a typical cubic coordination can be given explicitly as  $D = a^2 v/6$ , where  $a$  is the lattice constant and  $v$ , the characteristic frequency of the longitudinal optical phonon that carries polaron through the lattice.

Parent  $\text{LaMnO}_3$  at high temperatures is an insulator with a cubic structure and becomes tetragonal due to distortions at low temperatures. Doping at a La site by Ca, Sr, Ba, Na and K and so forth leads to a decrease not only in the structural phase transition temperature but also in the overall behaviour of resistivity. However, for optimized doped  $x \cong 0.3$ , the material is still insulating (at about room temperature and higher) and the resistivity is much higher than the Mott limit. The substitution at the La site by divalent (monovalent) ions changes the valence of the Mn site as outer Mn  $d$ -orbital shows two-fold degeneration, and the result is Jahn–Teller (breathing type) distortion of the oxygen octahedra focused at each of the Mn-occupied (unoccupied) sites. The energy required for the formation of a local lattice distortion is about 0.6 eV per site. Identifying a strong electron–phonon coupling and hence polaronic transport is essential in the doped materials. At high temperatures, the Jahn–Teller distortions are decorated but do not disappear.

On the other hand, the double-exchange mechanism shows that the oxygen ion is closed shell and supports hopping. In a true sense, an electron jumps onto a Mn ion on the right simultaneously with an electron hopping onto the O ion from the Mn on the left. Henceforth, in the double hopping, both hopping electrons should have the same spin via the oxygen ( $\text{O}^{2-}$ ) ions. Following Hund’s rule, the  $\text{Mn}^{3+}$  and  $\text{Mn}^{4+}$  ions should have the electron in parallel spin moments for hopping. This mechanism connects the parallel alignment of men moments (ferromagnetism) with hopping of carriers (metallic conduction). Thus an effective positive exchange coupling induced by the carriers was known as double exchange.

Actually, the lattice vibration of O ions essentially pushes the electrons towards vacant states in the Mn ion

inducing a local distortion of the lattice. Such self-trapping of the charge carriers is substantially above the Curie temperature. However, below the Curie temperature, the self-trapping disappears because the bandwidth broadens and the electrons are much more mobile. It is inferred that at high temperature, the effective positive exchange coupling induced by the carriers does not solely contribute to the resistivity and that a strong electron–phonon interaction arising from the Jahn–Teller splitting of the outer Mn *d* level is essentially required [38–40].

## Discussion and analysis of results

Any discussion of the mixed-valent oxides necessitates the knowledge of the structural aspects, and this is particularly true of the calculations reviewed here. Also, applying the available information on the developed theory inevitably entails certain complications, and one has to find suitable data that vary from technique to technique. Special attention is paid in this approach to address the issue whether long-range or short-range interactions are at the origin of the substantial properties of the monovalent K-doped manganites. The formulated effective inter-ionic interaction potential (EIoIP) with the long-range Coulomb interaction, van der Waals (vdW) interaction and the short-range repulsive interaction up to second-neighbour ions within the Hafemeister and Flygare approach is employed to estimate temperature-dependent resistivity for temperatures less than metal–insulator transition. We first elaborate the main findings and motivate them by simple physical arguments.

The present investigation concerns with electron–phonon scattering and theoretically analysed within the framework of the classical electron–phonon model of resistivity, i.e. the Bloch–Grüneisen (BG) model, as a dominating process for electrical resistivity. We first retrace the experimental data with  $\rho_0$  as the free parameter,

and then contribution from acoustic and optical phonons together with the residual resistivity is compared to the reported data and the difference is analysed in the light of electron–electron and electron–magnon scattering mechanisms. The above discussion of manganites needs an extremely accurate knowledge of the structural and transport parameters involved in either the metallic or semi-conducting state and this is particularly true for the calculation documented below. For the analysis of transport properties, it is necessary to know the real value of some physical parameters, which actually govern resistivity behaviour, however, they vary from technique to technique as well as the probe employed for characterizations. The effective interionic potential is constructed in an easily generalizable manner.

We have thus studied structural properties in an ordered way. The values of Debye and Einstein temperatures have been computed using the values of the two model parameters, namely range ( $\rho$ ) and hardness ( $b$ ), for a pair such as La/Ca/K–O and Mn–O, which have been evaluated from the equilibrium distance [41–43] and bulk modulus [44]. We first deduced the individual and overall vdW coefficients from the variational method [27], which are listed in Table 1. The material parameters such as hardness ( $b$ ) and range parameters ( $\rho$ ) as functions of doping concentration ( $x$ ) are obtained from the equilibrium distance and the bulk modulus using the equilibrium conditions. Within the continuum model, we notice that the hardness parameter ( $b_1$  and  $b_2$ ) increases and the range parameter ( $\rho_1$  and  $\rho_2$ ) decreases with the increased K doping concentration ( $x$ ) in doped  $\text{La}_{0.7}\text{Ca}_{0.3-x}\text{K}_x\text{MnO}_3$ . The input data along with their relevant references and the model parameters are given in Table 2.

Deduced values of second-order elastic constants  $C_{11}$ ,  $C_{12}$  and  $C_{44}$  are 9.655 (9.729), 4.816 (4.89) and 3.598 (3.667)  $10^{12}$  Dyne  $\text{cm}^{-2}$ , respectively for  $x = 0.05$  (0.1). Using Eq. (21), we find the force

**Table 1** Van der Waals coefficients of  $\text{La}_{0.7}\text{Ca}_{0.3-x}\text{K}_x\text{MnO}_3$  ( $x = 0.05, 0.1$ ) ( $c_{ij}$  in units of  $10^{-60}$  ergcm<sup>6</sup> and  $d_{ij}$  in unit of  $10^{-76}$  ergcm<sup>8</sup>)

		$c_{ii}$	$c_{ij}$	$c_{jj}$	$C$	$d_{ii}$	$d_{ij}$	$d_{jj}$	$D$
$x = 0.05$	Mn–O	120.1	180.3	270.8	1543	131.5	193.36	284.11	1355
	La/Ca/K–O	194.2	201.6	269.9	1750	547.6	446.0	284.10	3074
$x = 0.1$	La/Ca/K–O	197.5	203.0	269.1	1761	552.1	448.5	284.10	3091

**Table 2** Input crystal data and model parameters for  $\text{La}_{0.7}\text{Ca}_{0.3-x}\text{K}_x\text{MnO}_3$  ( $x = 0.05, 0.1$ )

		Input parameters			$B_T$ (GPa)	Model parameters	
		$r_i$ (Å)	$r_j$ (Å)	$r_0$ (Å)		$b(10^{-12}$ erg)	$\rho(10^{-1}$ Å)
$x = 0.05$	Mn–O	0.660 [43]	1.32 [43]	1.946 [41]	179 [44]	3.712	0.336
	La/Ca/K–O	1.223 [43]	1.32 [43]	2.881 [42]	179 [44]	3.162	0.214
$x = 0.1$	Mn–O	0.660 [43]	1.32 [43]	1.942 [41]	179 [44]	3.692	0.335
	La/Ca/K–O	1.242 [43]	1.32 [43]	2.881 [42]	179 [44]	2.712	0.218



constant,  $\kappa$ , accounting for long-range Coulomb interaction, van der Waals (vdW) interaction and the short-range repulsive interaction up to second-neighbour ions as  $3.755 (3.776) \times 10^5 \text{ gs}^{-2}$  for  $x = 0.05 (0.1)$ , respectively. With these parameters, the Debye frequency is estimated as 41.5 (41.8) meV for  $x = 0.05 (0.1)$ , respectively.

The Debye temperature plays an important role in the study of a large number of solid-state problems involving lattice vibrations because at this temperature, nearly all modes of vibrations in a solid are excited. It is clear that Debye frequencies are found to increase with  $x$ , as  $A$ -site radius varies and the observed behaviour might be due to structural transition and decrease in the Mn–O distance as a result of substitution of a  $\text{K}^+$  ion. The size of the  $\text{K}^+$  ion is larger than those of the  $\text{La}^+$  and  $\text{Ca}^+$  ions, which in turn creates more structural distortions in the lattice. Because of this, there is a change in Mn–O bond distance. This leads to affect the DE interaction resulting in increase in Debye frequency. We attempt to analyse our results in the framework of DE interaction with electron–lattice interaction. Therefore, when La site is substituted by Ca and K, the Mn–O distance decreases resulting in increase in  $\theta_D$  i.e. hardening of lattice. Henceforth, it suggests that increased hole doping drives the system effectively towards the weak electron–phonon coupling region. A similar behaviour is found for  $\text{La}_{1-x}\text{A}_x\text{MnO}_3$  when  $A$ -site is substituted for Na, K [45, 46].

We must mention that these computed values for  $\text{La}_{0.7}\text{Ca}_{0.3-x}\text{K}_x\text{MnO}_3$  for  $x = 0.05 (0.1)$  could not be compared due to the lack of experimental data. However, the computed values of Debye and Einstein temperatures for  $\text{La}_{1-x}\text{Na}_x\text{MnO}_3$  manganites following the EIoIP approach yield consistent results [47–49] with the available experimental results. Furthermore, the optical phonon mode is obtained as  $\omega_{TO} \approx 65.8 (65.7) \text{ meV}$  and  $\omega_{LO} \approx 68.8 (68.7) \text{ meV}$  for  $x = 0.05 (0.1)$ , respectively, consistent with the Raman spectroscopy results [4]. Optical Phonon modes shift towards a lower side with doped element. The La/Ca/K–O and Mn–O bonds govern these modes. If mode frequency is governed by local factors, such as the force constant and ionic mass of the substitutive elements as well, it will be proportional to  $(k/M)^{1/2}$ , where  $k$  is the force constant and  $M$  is the reduced mass [50]. The valence and ionic radius of  $\text{Ca}^{2+}$ ,  $\text{K}^+$  ions are different to those of  $\text{La}^{3+}$  ion. Therefore,  $k$  force constant and the mass of substitutive ion may cause a change in mode frequency. Analogous to that of  $\text{Nd}_{1-x}\text{Sr}_x\text{MnO}_3$  [37], substitution of  $\text{K}^+$  ion shows phonon softening with  $x$ . The average mass of the  $A$ -site and ionic radii affect the normal modes related to the La–O and Mn–O bonds; phonon modes shift gradually to lower mode frequencies with the doping concentration.

It is true that the two-orbital model based on Wannier functions predicts the electronic states such as charge ordering in manganites. It is pointed that the Wannier function approach of the electronic problem is useful for the description of electron dynamics following semi-classical theory as well as the magnetic interactions in solids [52]. In the present investigation, we do not intend to discuss the electron dynamics as well as the magnetic interactions but focus on determining the acoustic (optical) phonon frequency to estimate the electron–phonon contribution of resistivity in the ferromagnetic metallic phase.

The developed effective interionic interaction potential takes care of the interactions between a pair such as Mn–O and La/Ca/K–O. The interactions thus are attractive Coulomb, and van der Waals (vdW) as well as short-range overlap repulsive interaction following Hafemeister and Flygare type potential. The advantage of using this potential is that it takes care of the number of nearest (next nearest) ions, the valence, and the number of outermost electrons in the anions (cations), respectively. Thus it takes care of the structural parameters that yield an approximately correct description of the interactions between a pair such as Mn–O and La/Ca/K–O. Henceforth, we are able to estimate the acoustic (optical) phonon frequency consistent with the Raman measurements to estimate the electron–phonon contribution of resistivity.

The elastic parameters are determined using a mean field approximation with emphasis on Mn–O bond lengths and evaluated Mn–Mn and Mn–O force constants for the lattice distortions [38–40]. On the other hand, in the present model, we have considered both Mn–O and La/Ca/K–O bond lengths to obtain the Mn–O, La/Ca/K–O and the total force constants for strong electron–phonon interaction. The interionic interaction between a pair such as Mn–O and La/Ca/K–O enables us to find the total force constant with consistent Debye and Einstein temperatures.

The transport mechanism of the  $\text{La}_{0.7}\text{Ca}_{0.3-x}\text{K}_x\text{MnO}_3$  for ( $x = 0.05 (0.1)$ ) in the intermediate-temperature FM region below  $T_M$  is studied with the electron–phonon interaction to investigate the metallic behaviour of  $\rho(T)$ . Figures 1 and 2 illustrate the results of temperature dependence of resistivity with the electron–phonon interaction from Eq. (31) with our earlier choice of  $\theta_D = 485 (489) \text{ K}$  and  $\theta_E = 805 (808) \text{ K}$  for  $x = 0.05 (0.1)$ . The contributions of acoustic and optical phonon towards resistivity are clubbed, and the resultant resistivity is exponential at low temperatures and nearly linear at high temperatures until transition temperature. The coefficients  $A_{ac}$  ( $A_{op}$ ) as functions of doping concentration are shown in Table 3.

Given the numbers for coefficients ( $A_{ac}$  and  $A_{op}$ ) that emerge from the analysis, it seems fair to conclude that the contribution from acoustic and optical phonons are

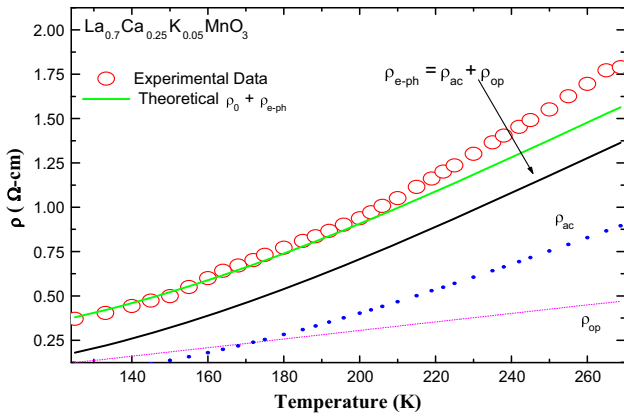


**Fig. 1** Variation of  $\rho_{e-ph}$  with temperature, the contribution of acoustic phonon  $\rho_{ac}$  as well as of optical phonon  $\rho_{op}$  to the resistivity for sample  $\text{La}_{0.7}\text{Ca}_{0.25}\text{K}_{0.05}\text{MnO}_3$ . *Hollow circles* represent the experimental data [5]

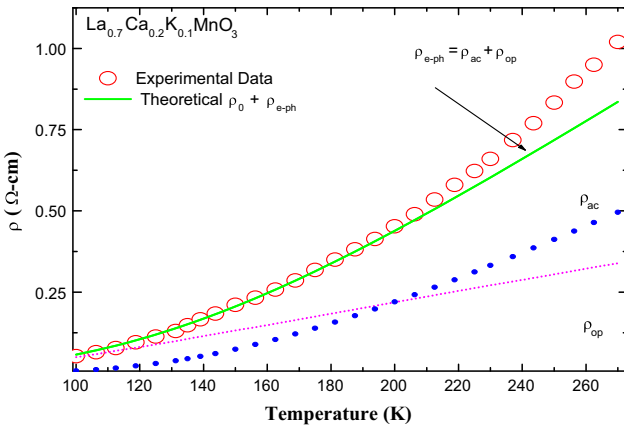


**Fig. 2** Variation of  $\rho_{e-ph}$  with temperature, the contribution of acoustic phonon  $\rho_{ac}$  as well as of optical phonon  $\rho_{op}$  to the resistivity for sample  $\text{La}_{0.7}\text{Ca}_{0.2}\text{K}_{0.1}\text{MnO}_3$ . *Hollow circles* represent the experimental data [5]

**Table 3** The fitting parameters obtained from the Bloch–Gruneisen model for  $\text{La}_{0.7}\text{Ca}_{0.3-x}\text{K}_x\text{MnO}_3$  ( $x = 0.05, 0.1$ )

	$\omega_D$ (meV)	$\omega_{TO}$ (meV)	$\omega_{LO}$ (meV)	$A_{ac}$	$A_{op}$
$x = 0.05$	41.5	65.8	68.8	$2.08 \times 10^{-3}$	$6.7 \times 10^{-3}$
$x = 0.1$	41.8	65.7	68.7	$1.5 \times 10^{-3}$	$3.69 \times 10^{-3}$

significant in both samples, while in  $\text{La}_{0.7}\text{Ca}_{0.25}\text{K}_{0.05}\text{MnO}_3$ , contribution of acoustic phonon is more for electron–phonon resistivity and in the case of  $\text{La}_{0.7}\text{Ca}_{0.2}\text{K}_{0.1}\text{MnO}_3$ , there is large contribution of optical phonon. In spite of the difference in contribution from both phonons, both samples show electron–phonon interaction up to nearly same temperature range. Therefore, this electron–phonon interaction inherent in K-doped  $\text{La}_{0.7}\text{Ca}_{0.3}\text{MnO}_3$  sample may be due to possible larger lattice distortions provoked by the K ions. It

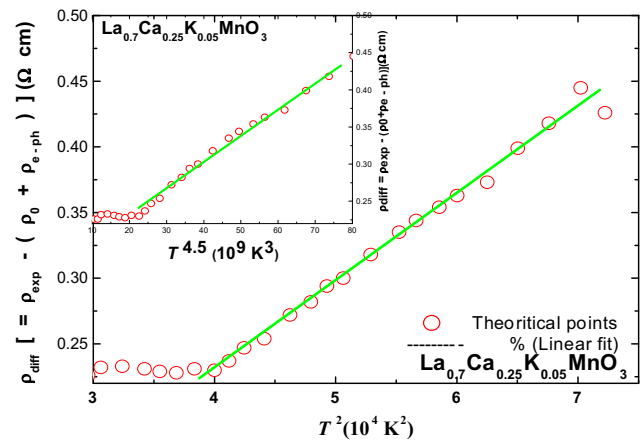


**Fig. 3** Variation of  $\rho_{diff}$ . [ $= \rho_{exp} - \{\rho_0 + \rho_{e-ph} (= \rho_{ac} + \rho_{op})\}$ ] with  $T^2$  of  $\text{La}_{0.7}\text{Ca}_{0.25}\text{K}_{0.05}\text{MnO}_3$ . The *inset* shows variation of  $\rho_{diff}$ . [ $= \rho_{exp} - \{\rho_0 + \rho_{e-ph} (= \rho_{ac} + \rho_{op})\}$ ] with  $T^{4.5}$

is noticed that the electron–phonon along with residual resistivity partially retraces the metallic resistivity behaviour of  $\text{La}_{0.7}\text{Ca}_{0.25}\text{K}_{0.05}\text{MnO}_3$  and  $\text{La}_{0.7}\text{Ca}_{0.2}\text{K}_{0.1}\text{MnO}_3$  manganites, and other temperature-dependent mechanisms such as electron–electron and electron–magnon scattering should also be invoked.

We have discussed only how electron–phonon interaction retraces approximately the resistivity behaviour, yet our goal is to determine the manner in which other interactions modify the electrical resistivity. The additional term due to electron–electron contribution was required in understanding the resistivity behaviour, as extensive attempts to fit the data with residual resistivity and phonon resistivity were unsuccessful. It is noteworthy to comment that in conventional metals, the electron–electron contribution to the resistivity can at best be seen only at very low temperatures, due to its small magnitude in comparison with the phonon contribution.

The temperature-dependent resistivity,  $\rho_{diff}$ . [ $= \rho_{exp} - \{\rho_0 + \rho_{e-ph} (= \rho_{ac} + \rho_{op})\}$ ], is proportional to power temperature ( $T^2$ ) from 198 to 245 K for  $\text{La}_{0.7}\text{Ca}_{0.25}\text{K}_{0.05}\text{MnO}_3$  and 200 to 250 K for  $\text{La}_{0.7}\text{Ca}_{0.2}\text{K}_{0.1}\text{MnO}_3$  as shown in Figs. 3 and 4. This infers that electron–electron scattering is also a dominant process for resistivity of  $\text{La}_{0.7}\text{Ca}_{0.25}\text{K}_{0.05}\text{MnO}_3$  and  $\text{La}_{0.7}\text{Ca}_{0.2}\text{K}_{0.1}\text{MnO}_3$ . The fitting results indicate that K doping significantly decreases the electron–phonon interaction, which favours the movement of the charge carriers. Slight deviations need an additional scattering mechanism for consistent explanation of the metallic behaviour of resistivity. At high temperatures, electron scattering is isotropic due to the predominance of electron–phonon scattering, which is nearly isotropic at high temperatures.

The inset of Figs. 3 and 4 shows the fitting in terms of  $T^{4.5}$  behaviour. It is noticed that  $T^{4.5}$  behaviour

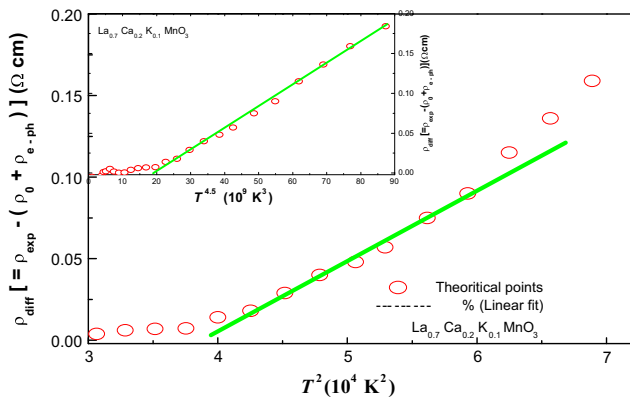


**Fig. 4** Variation of  $\rho_{diff.} [= \rho_{exp.} - \{\rho_0 + \rho_{e-ph} (= \rho_{ac} + \rho_{op})\}]$  with  $T^2$  of  $\text{La}_{0.7}\text{Ca}_{0.2}\text{K}_{0.1}\text{MnO}_3$ . The inset shows variation of  $\rho_{diff.} [= \rho_{exp.} - \{\rho_0 + \rho_{e-ph} (= \rho_{ac} + \rho_{op})\}]$  with  $T^{4.5}$

remarkably increases with increasing K doping level, implying that the electron–magnon scattering enhances with the increase in K doping. Thus, the transport mechanism in the near-transition temperature region can be attributed to the electron–electron and electron–magnon scattering, which further demonstrates that the metallic region lies in the FM phase. For the present temperature region, the contribution of a phonon is usually ignored due to the weak vibration of crystal lattice.

For hole-doped manganites, an additional  $T^{4.5}$  contribution as a result of electron–magnon scattering process is argued to be essential [53]. In the recent past, we have also noticed that the spin wave scattering in the FM phase is important in discussing the electrical resistivity behaviour of hole-doped  $\text{La}_{0.91}\text{Rb}_{0.06}\text{Mn}_{0.94}\text{O}_3$  manganites [11–13]. We admit that in the higher temperature limit, the difference can be predicted linearly with  $T^{4.5}$  in accordance with the electron–magnon scattering in the double-exchange process. The feature of  $T^{4.5}$  temperature dependence of  $\rho_{diff.}$  is consistent with the quantum theory of two-magnon scattering [53] and is valid for half-metallic ferromagnets. Consequently, besides electron–phonon and electron–electron interaction, another possibility for the changes in carrier density arose due to the presence of spin waves in the metallic system and is caused by spin wave scattering.

We shall now address the metallic behaviour of doped manganites. If the high-frequency phonon modes are indeed strongly coupling with charge carriers, the effective mass of the carriers should be substantially enhanced. The Fermi energy can be known from the reported values of thermoelectric power using  $\varepsilon_F = -\pi^2 k_B^2 T / [3 |e| S_c^{diff.}(T)]$ , we find  $\varepsilon_F \cong 0.677$  (0.897) eV for  $\text{La}_{0.7}\text{Ca}_{0.25}\text{K}_{0.05}\text{MnO}_3$  ( $\text{La}_{0.7}\text{Ca}_{0.2}\text{K}_{0.1}\text{MnO}_3$ ), respectively [2]. Deduced Fermi energy corresponds to the density of states  $N(\varepsilon_F) \cong 4.019$  ( $6.371$ )  $\times 10^{19} \text{ eV}^{-1} \text{ cm}^{-3}$  for doping concentration,  $x = 0.05$  (0.1), respectively.

The density of states at Fermi level found to increase with K doping. The observed behaviour can be explained on the basis of Mn valence present in these samples. The K doping in  $\text{La}_{0.7}\text{Ca}_{0.3}\text{MnO}_3$  showed increase in  $\text{Mn}^{4+}$  ions that favour double exchange between Mn ions. As a consequence, the increase in  $N(\varepsilon_F)$  suggested an appreciable increase in the number of charge carriers accompanied by increase of conductivity of K doping, which is further supported by resistivity data [5]. The density of states in turn yields the electronic specific heat coefficient using  $\gamma = (\pi k_B)^2 N(\varepsilon_F) / 3$ . We thus find the values of  $\gamma = 3.523$  (5.585)  $\text{mJmol}^{-1} \text{ K}^{-2}$  consistent with the  $\gamma$  values in hole-doped divalent manganites [54]. These could not be compared due to the lack of experimental data on  $\text{La}_{0.7}\text{Ca}_{0.3-x}\text{K}_x\text{MnO}_3$  monovalent manganites.

The effective mass of the carrier along the conducting Mn–O plane is deduced from the electronic specific heat coefficient  $\gamma$ , using  $m^* = 3\hbar^2 \pi \gamma d / k_B^2$ . Using the MnO distance,  $d$ , of 7.7301 (5.4662) Å [41], we find  $m^* = 2.031$  (2.514)  $m_e$ . The estimated electron parameters for  $\text{La}_{0.7}\text{Ca}_{0.25}\text{K}_{0.05}\text{MnO}_3$  ( $\text{La}_{0.7}\text{Ca}_{0.2}\text{K}_{0.1}\text{MnO}_3$ ) are the Fermi wave vector  $k_F = 3.581$  (4.586)  $\times 10^7 \text{ cm}^{-1}$ , the Fermi velocity  $v_F = 2.035$  (2.105)  $\times 10^7 \text{ cms}^{-1}$  and the plasma frequency  $\omega_p = 1.406$  (1.831) eV. We stress that the effects induced by electron correlations and mass renormalizations by electron–electron interactions are crucial in magnetic systems such as doped manganites [55–65].

In usual conventional metals, electron–phonon scattering is mathematically identical to conventional impurity scattering and leads to a resistivity proportional to  $(v_F^2)^{-1}$  where  $l$  is the mean free path. The mean free path in this approximation is usually related to the Fermi velocity and is estimated following  $l = v_F \tau$ . We find  $l$  to be about 3.058 (3.072) Å, for  $x = 0.05$  (0.1), respectively. We follow the Drude relation,  $\tau^{-1} = \rho_0 \omega_p^2 / 4\pi$  to obtain  $\tau^{-1} = 6.664$  ( $6.852$ )  $\times 10^{15} \text{ s}^{-1}$ . We must mention that the residual resistance obtained for nominally the same compositions may vary significantly for different groups of compounds. It remains unclear whether  $\rho_0$  only characterizes the sample’s quality or if there is an intrinsic component in the residual resistivity [66]. For the Sr-doped manganites, the resistivity data in the crystalline films yield  $\rho_0$  as low as  $10^{-5} \Omega \text{ cm}$  and are in the range of typical metallic conductors [67]. We notice that the  $\text{La}_{0.7}\text{Ca}_{0.25}\text{K}_{0.05}\text{MnO}_3$  ( $\text{La}_{0.7}\text{Ca}_{0.2}\text{K}_{0.1}\text{MnO}_3$ ) manganites are good metals as the product  $\varepsilon_F \tau > 1$ .

The electron correlations in view of the mass enhancement effect in narrow band materials are important in doped manganites. The phenomenon that mass enhanced with substituting ion can be interpreted as follows: substitution stimulate manganese content and these  $\text{Mn}^{4+}$  ions induced an increase in bending of Mn–O–Mn bond angle, in this manner narrowing band width and enhancing the

effective mass [68]. We notice that enhanced electron mass  $m^* = 2.031$  (2.514)  $m_e$  in  $\text{La}_{0.7}\text{Ca}_{0.3-x}\text{K}_x\text{MnO}_3$  leads to the reduced plasma frequency, and hence the reduced zero temperature elastic scattering rate in comparison to conventional metals. It is perhaps worth noticing that, in hole-doped manganites, the scattering rate at low temperatures is of the order of  $10^{15} \text{ s}^{-1}$  [55–65]. Furthermore, the Mott–Ioffe–Regel criterion for metallic conductivity is valid, as the deduced mean free path is larger than the Mn–O bond length. The use of the Bloch–Grüneisen expression in estimating the electron–phonon contributions is thus validated as the product  $k_F l > 1$ .

The monovalent (K)-doped  $\text{La}_{0.7}\text{Ca}_{0.3}\text{MnO}_3$  manganites thus illustrate a metallic behaviour below 269 (275) K a temperature  $T_{MI}$  for  $x = 0.05$  (0.1), respectively. The metal–insulator transition temperature  $T_{MI}$  increases with the K doping concentration. With increased doping,  $\text{La}_{0.7}\text{Ca}_{0.3-x}\text{K}_x\text{MnO}_3$  manganites behave as good metal and this is attributed to the fact that there are twice as many  $\text{Mn}^{4+}$  ions as there are K ions and each of this  $\text{Mn}^{4+}$  will contribute a hopping hole. Consequently, K doping will cause increase in the number of charge carriers and hence resistivity will be decreased.

The effects of the grain-boundary-induced lattice disorder on the resistivity in  $\text{Sm}_{0.55}\text{Sr}_{0.45}\text{MnO}_3$  at temperatures near the metal–insulator transition have earlier been emphasized [69]. The low temperature resistivity data ( $T \leq 75$  K) of the  $\text{SmSrMnO}$  were successfully fitted using the relation  $\rho = \rho_0 + \rho_2 T^2 + \rho_5 T^5$  with  $\rho_0$  as the residual resistivity and  $\rho_2$  and  $\rho_5$  are the electron–electron and the electron–phonon scattering coefficients, respectively. It is further noticed that in this temperature range, the disorder does not affect the temperature dependence of  $\rho$ ; however, it causes an increase in the coefficients  $\rho_0$ ,  $\rho_2$  and  $\rho_5$  by two orders of magnitude.

In contrast to electron–phonon scattering as the source of resistivity in ferromagnetic metallic (FM) state, the angle-resolved photoemission spectroscopy data for the bilayer manganite  $\text{La}_{1.2}\text{Sr}_{1.8}\text{Mn}_2\text{O}_7$  identify a coherent polaronic metallic ground state below metal–insulator transition. The FM state is a polaronic metal with a strong anisotropic character of the electronic excitations, strikingly similar to the pseudogap phases in heavily underdoped cuprate high-temperature superconductors such as Bi 2212. A strong mass enhancement and a small renormalization factor are found to account for the metallic properties [70, 71]. The temperature dependence of resistivity in the metallic state is intimately related to polaronic metallic ground state and the insulator-to-metallic state can be attributed to the polaron coherence condensation process acting in concert with the double-exchange mechanism. We may comment that the present theory finds an enhanced mass of holes as carriers [ $m^* = 2.031$  (2.514)  $m_e$

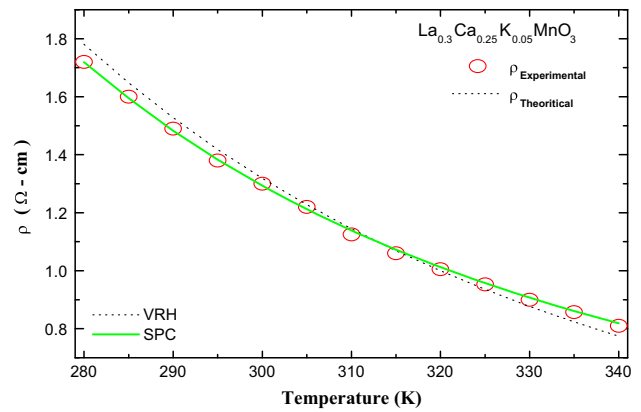


**Fig. 5** Variation of  $\rho$  for high-temperature region,  $T > T_{MI}$  Open circles are the experimental data taken from Sdiri et al. [5]. Solid line is the fitting by Small Polaron conduction model and dashed line is from the Variable range hopping model of  $\text{La}_{0.7}\text{Ca}_{0.25}\text{K}_{0.05}\text{MnO}_3$

for  $\text{La}_{0.7}\text{Ca}_{0.25}\text{K}_{0.05}\text{MnO}_3$  ( $\text{La}_{0.7}\text{Ca}_{0.2}\text{K}_{0.1}\text{MnO}_3$ )] from the residual resistivity to validate the Mott–Ioffe–Regel criterion. However, a detailed analysis is required to understand the polaronic metallic state in the ferromagnetic phase and the condensation process analogous to under-doped cuprate high-temperature superconductors.

Let us now discuss the semi-conducting behaviour of resistivity data in the high-temperature region and paramagnetic semi-conducting state ( $T > T_{MI}$ ). We have computed the temperature-dependent resistivity of  $\text{La}_{0.7}\text{Ca}_{0.3-x}\text{K}_x\text{MnO}_3$  ( $x = 0.05, 0.1$ ) using variable range hopping (VRH) and adiabatic small polaron conduction (SPC) model. Keeping in mind that the charge carrier motion is faster than the lattice vibrations in the adiabatic regime, the nearest-neighbour hopping of a small polaron leads to mobility with a thermally activated form.

To understand the nature of electrical conduction behaviour in K-doped  $\text{La}_{1-x}\text{Ca}_x\text{MnO}_3$  materials, we have analysed the resistivity data using Mott’s variable range hopping VRH model [14]. Originally in the VRH theory, there is a competition between the potential energy and the hopping distance of electrons. Figures 5 and 6 show the plots of high-temperature resistivity  $\rho$  as a function of temperature  $T$  revealing good concurrence with VRH model [Eq. (32)]. The values of fitting parameters obtained from the fit of the high-temperature resistivity of  $\text{La}_{0.7}\text{Ca}_{0.25}\text{K}_{0.05}\text{MnO}_3$  ( $\text{La}_{0.7}\text{Ca}_{0.2}\text{K}_{0.1}\text{MnO}_3$ ) by the VRH model are  $\rho_{oh} = 0.04069$  ( $0.7 \times 10^{-6}$ )  $\Omega \text{ cm}$  and  $T_0 = 2.683 \times 10^6$  ( $2.158 \times 10^6$ ) K. The fitted value of  $T_0$  and the localization length or the average hopping distance  $\{a = 4.6 \text{ \AA}$  [15]} yield the density of states at the Fermi level,  $N(\varepsilon_F)$ , of the order of  $0.799$  ( $9.943$ )  $\times 10^{20} \text{ eV}^{-1} \text{ cm}^{-3}$ . The above sets of values are consistent with the fitting parameters for  $\text{Nd}_{0.33}\text{Ln}_{0.34}\text{Sr}_{0.33}\text{MnO}_3$  [72].

To have a cross check, we use the thermo electric power measurement to calculate experimental value of the density

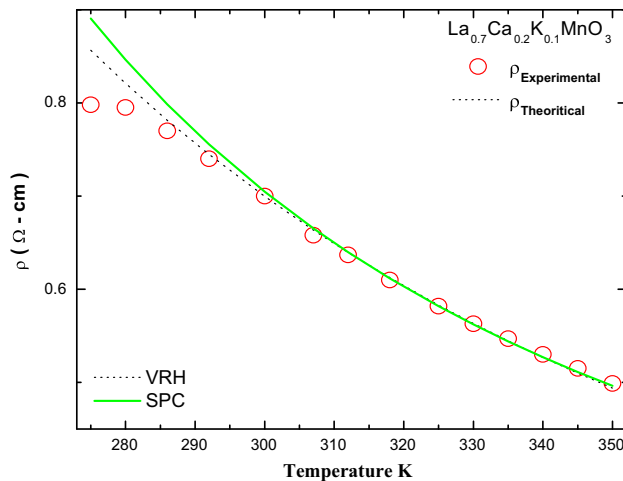


**Fig. 6** Variation of  $\rho$  for high-temperature region,  $T > T_{MI}$ . Open circles are the experimental data taken from Sdiri et al. [5]. Solid line is the fitting by Small Polaron conduction model and dashed line is from the Variable range hopping model of  $\text{La}_{0.7}\text{Ca}_{0.2}\text{K}_{0.1}\text{MnO}_3$

of states at the Fermi level [2]. Deduced density of states  $N(\epsilon_F) \cong 4.019 (6.123) \times 10^{19} \text{ eV}^{-1} \text{ cm}^{-3}$  for doping concentration,  $x = 0.05 (0.1)$ , respectively. We comment that the value of density of states at the Fermi level obtained from semi-conducting resistivity fit using VRH is higher by an order as obtained from thermoelectric power measurements. This unphysical result leads us to argue that the VRH model is not a proper choice to describe resistivity behaviour in the high-temperature region,  $T > T_{MI}$  for  $\text{La}_{0.7}\text{Ca}_{0.3-x}\text{K}_x\text{MnO}_3$  ( $x = 0.05, 0.1$ ). Earlier, Mott and Davies argued that the VRH model is applicable only for the temperature region ( $T_{MI} < T < \theta_D/2$ ) in doped semi-conductors [73]. The above is true for K-doped manganites  $\text{La}_{0.7}\text{Ca}_{0.3-x}\text{K}_x\text{MnO}_3$  ( $x = 0.05, 0.1$ ) with  $T_{MI} \cong 269$  (275) K and  $\theta_D \cong 485$  (486) K.

The above discrepancy in density of states at the Fermi level might be due to spin-dependent potential in doped manganites [15]. Quite generally, in strongly correlated electron systems such as mixed-valent manganites, the carrier hopping is always of a variable-range type at low temperature. As at low temperatures, the thermal energy ( $k_B T$ ) is insufficient to allow electrons to hop to their nearest neighbours. However, electrons conveniently hop to farther neighbours to find a smaller potential difference, and there is a competition between the potential energy difference and the distance electrons can hop. On the other hand, at higher temperatures, the electron conduction is due to the activation above the mobility edge. The above results are consistent with previous work [11, 47–49].

We have further used the adiabatic small polaron conduction (SPC) model for the analysis of resistivity behaviour for high temperature. Charge carriers in the insulating region, above  $T_{MI}$ , are not itinerant and thermally activated

**Table 4** Parameters obtained from the fitting of experimental data using VRH and SPC model

	$T_0$ $10^7$ (K)	$N(\epsilon_F) 10^{20}$ ( $\text{eV}^{-1} \text{ cm}^{-3}$ )	$D 10^{-2}$ ( $\text{cm}^2 \text{ s}^{-1}$ )	$\rho_{os} 10^{-5}$ ( $\Omega \text{ cm K}^{-1}$ )	$E_p$ (meV)
$x = 0.05$	2.683	0.799	5.2	3.049	128
$x = 0.1$	0.215	9.943	5.3	6.872	91

carriers (polaron) controlled the transport mechanism. It is argued that the conductivity of the high-temperature ( $T > T_{MI}$ ) PM insulating state is attributed to the hopping motion of self-trapped small polaron. To elucidate the nature of the charge transport mechanism in this high-temperature region,  $\rho$  has been plotted as a function of  $T$  in Figs. 5 and 6. The good linear fits reveal that the conduction in the PM semi-conducting region obeys the small polaron hopping model. The activation energy obtained from fitting of experimental data is given in Table 4. The decrease in  $E_p$  is attributed to the increase in the number of charged carrier caused by K addition.

We have first determined the diffusion coefficient using the lattice constant; the longitudinal optical phonon frequency and polaron formation energy are enlisted in Table 4. The decrease in  $E_p$  is also attributed to the effect of cationic disorder by the larger size of the monovalent ion  $\text{K}^+$  compared to  $\text{La}^{3+}$  and  $\text{Ca}^{2+}$  ions. In addition to the effect of cationic disorder, change in Mn valance effectively leads to structural change. K doping provoked  $\text{Mn}^{4+}$  ions consequently with increasing  $x$  there is decrease in Mn–O–Mn bond angle substantial increases density of states at Fermi level and enhancing effective mass of charge carrier due to this effective band gap decreases. Therefore, activation energy values decrease with  $x$ . It is interesting to note that the sample with the higher  $\text{Mn}^{4+}$  content shows the lower  $E_p$  value.

The computed values of  $E_p$  for  $\text{La}_{0.7}\text{Ca}_{0.3-x}\text{K}_x\text{MnO}_3$  for ( $x = 0.05, 0.1$ ) could not be compared due to the lack of experimental data. However, the polaron formation energy ranges from 110 to 160 meV in  $\text{La}_{1-x}\text{Ca}_x\text{MnO}_3$  ( $0 \leq x \leq 0.5$ ) and ranges from 50 to 110 meV in  $\text{La}_{1-x}\text{K}_x\text{MnO}_3$  ( $0 \leq x \leq 0.33$ ) [74–76]. The deduced value of the  $E_p$  lies between above range and it reveals that addition of K increases the carrier density. The fact that  $E_p$  gradually decreases for higher doping is due to the phonon softening effect on carrier transport owing to Jahn–Teller distortions in the K-doped  $\text{La}_{0.7-x}\text{Ca}_{0.3}\text{MnO}_3$ . Henceforth, above  $T_{MI}$ , the Jahn–Teller-type distortion present in the unit cell traps the charge carriers and gives rise to polarons. Hence, above  $T_{MI}$ , resistivity shows polaronic-type behaviour. We end up by commenting that the SPC model with realistic physical parameters successfully retraces the reported experimental behaviour ( $T > \theta_D/2$ ;  $T > T_{MI}$ ) of resistivity in doped manganites.

## Conclusion

The present investigations report the analysis of experimentally known behaviour of electrical resistivity in monovalent (K)-oped  $\text{La}_{0.7}\text{Ca}_{0.3}\text{MnO}_3$  manganites for metallic and semi-conducting states. For  $T < T_{MI}$  in the ferromagnetic metallic state, we have employed the electron–phonon interaction with the model phonon spectrum consisting of two parts: an acoustic branch of Debye type and optical mode with characteristic Einstein temperature. Debye and Einstein temperatures from the EIoIP within the Hafemeister and Flygare approach are deduced.

The proposed model may, in spite of its simple structure, provide a consistent account for the experimental fact, such as Debye and Einstein temperatures consistent with the specific heat and Raman spectroscopy measurements. It is emphasized that conclusions have been established only within the framework of single (longitudinal and transverse) optical phonon mode with a flat dispersion relation. It is due to the fact that substitution of a  $\text{K}^+$  ion creates more structural distortions in the lattice as a result of decrease in Mn–O bond distance, consequently affecting the DE interaction and thus resulting in increase in Debye frequency. Einstein temperatures were found to decrease with doping. This reduction is ascribed by the blue-shift of Optical Phonon modes, which are governed by the La/Ca/K–O and Mn–O bonds. The average mass of the A-site and ionic radii affects normal modes related to the La/Ca/K–O and Mn–O bonds; phonon modes are blue-shifted gradually with enhanced alkali metal K doping.

Signatures of different types of interaction terms as electron–phonon, electron–electron and electron–magnon are found to govern the transport mechanism in the low-temperature phase ( $T < T_{MI}$ ). The temperature-dependent resistivity data in this region, where the local ferromagnetic order is almost complete, have been successfully fitted with  $\rho = \rho_0 + \rho_{e-ph} + \rho_{e-e} (T^2) + \rho_{e-mag} (T^{4.5})$ . It is thus argued that apart from the resistivity due to domain, grain-boundary and the electron–phonon scattering, the electron–electron and electron–magnon scattering are essential for a complete description of the metallic behaviour of  $\text{La}_{0.7}\text{Ca}_{0.3-x}\text{K}_x\text{MnO}_3$  for ( $x = 0.05$ – $0.1$ ) manganites. However, the contribution of electron–phonon scattering appears similar in both samples and only contributions from acoustic and optical phonons are different. In this way, K doping impelled lattice distortion confirmed through electron–phonon contribution. The mean free path is larger than the Mn–O bond length, and the product  $k_{Fl} \geq 1$  and  $\varepsilon_F \tau > 1$  favours metallic conduction. Hence, it is appropriate to use the Bloch–Grüneisen expression in estimating the electron–phonon contributions at  $T < T_{MI}$ , and this is associated with the dynamic Jahn–Teller distortion, arising

from the local lattice distortion due to the strong electron–phonon coupling.

The resistivity data of semi-conducting state at high-temperature region,  $T > T_{MI}$ , is analysed using both the VRH and adiabatic SPC models. Deduced values of  $N(\varepsilon_F)$  are found to increase and this phenomenon is associated with Mn valence induced by K doping. The small polaron conduction model with realistic physical parameters consistently retraces the semi-conducting behaviour. The nearest-neighbour hopping of a small polaron leads to a mobility with a thermally activated form and successfully retraced the reported experimental curve in the paramagnetic phase.  $E_p$  gradually decreases which may be due to decreasing charge localization with doping and also from phonon softening effect on carrier transport owing to the Jahn–Teller distortions in the  $\text{La}_{0.7}\text{Ca}_{0.3-x}\text{K}_x\text{MnO}_3$ . Above  $T_{MI}$ , the Jahn–Teller-type distortion present in the unit cell traps the charge carriers and gives rise to polarons and for  $T > T_{MI}$ , the resistivity behaviour is indeed polaronic-type.

To an end, we comment that although we have provided a simple explanation of these effects, there is a clear need for good theoretical understanding of the resistivity behaviour in view of the formation of small polarons that may be of magnetic origin in manganites.

**Acknowledgments** The authors are thankful to UGC, New Delhi for financial assistance.

**Open Access** This article is distributed under the terms of the Creative Commons Attribution License which permits any use, distribution, and reproduction in any medium, provided the original author(s) and the source are credited.

## References

1. Malavasi, L., Mozzati, M.C., Ghigna, P., Azzoni, C.B., Flor, G.: Lattice disorder, electric properties, and magnetic behavior of  $\text{La}_{1-x}\text{Na}_x\text{MnO}_{3+\delta}$  manganites. *J. Phys. Chem. B* **107**, 2500–2505 (2003)
2. Bhattacharya, S., Pal, S., Mukherjee, R.K., Chaudhuri, B.K., Neeleshwar, S., Chen, Y.Y., Mollah, S., Yang, H.D.: Development of pulsed magnetic field and study of magnetotransport properties of K-doped  $\text{La}_{1-x}\text{Ca}_x\text{K}_y\text{MnO}_3$  CMR materials. *J. Magn. Magn. Mater.* **269**, 359–371 (2004)
3. Salamon, M.B., Jaime, M.: The physics of manganites: structure and transport. *Rev. Mod. Phys.* **73**, 583–628 (2001)
4. Bejar, M., Feki, H., Dhahri, E., Ellouze, M., Balli, M., Hlil, E.K.: Effects of substituting divalent by monovalent ion on the physical properties of  $\text{La}_{0.7}\text{Ca}_{0.3-x}\text{K}_x\text{MnO}_3$  compounds. *J. Magn. Magn. Mater.* **316**, 707–709 (2007)
5. Sdiri, N., Jemai, R., Bejar, M., Hussein, M., Khirouni, K., Dhahri, E., Mazen, S.: Electrical conductivity and dielectric analysis of the perovskite  $\text{La}_{0.7}\text{Ca}_{0.3-x}\text{K}_x\text{MnO}_3$  ( $x = 0.00, 0.05$  and  $0.10$ ). *Solid State Commun.* **148**, 577–581 (2008)
6. Kumar, S., Majumdar, P.: Singular effect of disorder on electronic transport in strongly coupled electron–phonon systems. *Phys. Rev. Lett.* **94**, 136601–136604 (2005)

7. Panwar, N., Pandya, D.K., Rao, A., Wu, K.K., Kaurav, N., Kuo, Y.K., Agarwal, S.K.: Electrical and thermal properties of  $\text{Pr}_{2/3}(\text{Ba}_{1-x}\text{Cs}_x)_{1/3}\text{MnO}_3$  manganites. *Eur. Phys. J. B* **65**, 179–186 (2008)
8. Chen, Z., Xu, Y., Su, Y., Cao, S., Zhang, J.: Resistivity minimum behavior and weak magnetic disorder characteristics in  $\text{La}_{2/3}\text{Ca}_{1/3}\text{MnO}_3$  manganites. *J. Supercond. Nov. Magn* **22**, 465–469 (2009)
9. Rozenberg, E.: Comment on ‘Resistivity Minimum Behavior and Weak Magnetic Disorder Characteristics in  $\text{La}_{2/3}\text{Ca}_{1/3}\text{MnO}_3$  Manganites’. *J. Supercond. Nov. Magn.* **23**, 183–186 (2010)
10. Alexandrov, A.S., Kornilovitch, P.B.: Mobile small polaron. *Phys. Rev. Lett.* **82**, 807–810 (1999)
11. Varshney, D., Dodiya, N.: Interpretation of metallic and semi-conducting temperature dependent resistivity of  $\text{La}_{0.91}\text{Rb}_{0.06}\text{Mn}_{0.94}\text{O}_3$  manganites. *Solid State Sci* **13**, 1623–1632 (2011)
12. Varshney, D., Dodiya, N.: Structural and magnetotransport studies of magnetic ion doping for monovalent-doped  $\text{LaMnO}_3$  manganites. *J. Mater. Res.* **29**, 1183–1198 (2014)
13. Varshney, D., Shaikh, M.W.: Substitutional effects on structural and magnetotransport properties of  $\text{La}_{0.85-x}\text{Sm}_x\text{K}_{0.15}\text{MnO}_3$  ( $x = 0.05, 0.1$  and  $0.15$ ). *J. Alloys Compds.* **589**, 558–567 (2014)
14. Snyder, G.J., Hiskes, R., Dicarolis, S., Beasley, M.R., Geballe, T.H.: Intrinsic electrical transport and magnetic properties of  $\text{La}_{0.67}\text{Ca}_{0.33}\text{MnO}_3$  and  $\text{La}_{0.67}\text{Sr}_{0.33}\text{MnO}_3$  MOCVD thin films and bulk material. *Phys. Rev. B* **53**, 14434–14444 (1996)
15. Viret, M., Ranno, L., Coey, J.M.D.: Magnetic localization in mixed-valence manganites. *Phys. Rev. B* **55**, 8067–8070 (1997)
16. Jaime, M., Hardner, H.T., Salamon, M.B., Rubinstein, M., Dorsey, P., Emin, D.: Hall-effect sign anomaly and small-polaron conduction in  $(\text{La}_{1-x}\text{Gd}_x\text{d})_{0.67}\text{Ca}_{0.33}\text{MnO}_3$ . *Phys. Rev. Lett.* **78**, 951–954 (1997)
17. Ang, R., Lu, W.J., Zhang, R.L., Zhao, B.C., Zhu, X.B., Song, W.H., Sun, Y.P.: Effects of Co doping in bilayered manganite  $\text{LaSr}_2\text{Mn}_2\text{O}_7$ : resistivity, thermoelectric power, and thermal conductivity. *Phys. Rev. B* **72**(184417), 1–8 (2005)
18. Hafemeister, D.W., Flygare, W.H.: Outer-shell overlap integral as a function of distance for halogen–halogen, halogen–alkali, and alkali–alkali ions in the alkali halide lattices. *J. Chem. Phys.* **43**(1965), 795–800 (1965)
19. Varshney, D., Joshi, G., Varshney, M., Shriya, S.: Pressure dependent elastic and structural (B3–B1) properties of Ga based monopnictides. *J. Alloys Compd.* **495**, 23–32 (2009)
20. Varshney, D., Joshi, G., Varshney, M., Shriya, S.: Pressure induced structural phase transition and elastic properties in B5b, AlSb, GaSb and InSb compounds. *Phys B* **405**, 1663–1676 (2010)
21. Varshney, D., Shriya, S., Varshney, M.: Study of pressure induced structural phase transition and elastic properties of lanthanum pnictides. *Eur. Phys. J. B* **85**, 241–272 (2012)
22. Varshney, D.: Mechanical and elastic properties of Europium mono-oxides and mono-chalcogenides ( $\text{EuX}$ ;  $X = \text{O}, \text{S}, \text{Se}, \text{Te}$ ), Europium: synthesis, characteristics and potential applications. In: Attia, M.S. (ed.) pp. 247–292. Nova Science Publication, New York (2013)
23. Varshney, D., Shriya, S.: Elastic, mechanical and thermodynamic properties at high pressures and temperatures of transition metal monocarbides. *Int. J. Refract. Metals Hard Mater.* **41**, 375–401 (2013)
24. Varshney, D., Joshi, G., Varshney, M., Shriya, S.: Pressure dependent elastic and structural (B3–B1) properties of Ga based monopnictides. *J. Alloys Compds.* **495**, 23–32 (2010)
25. Dodiya, N., Varshney, D.: Structural properties and Raman spectroscopy of rhombohedral  $\text{La}_{1-x}\text{Na}_x\text{MnO}_3$  with ( $0.075 \leq x \leq 0.15$ ). *J. Mol. Struct.* **2013**, 104–109 (1031)
26. Tosi, M.P.: Cohesion of ionic solids in the born model. *Solid State Phys.* **16**, 1–120 (1964)
27. Slater, J.C., Kirkwood, J.G.: The van der Waals forces in gases. *Phys. Rev.* **37**, 682–697 (1931)
28. Varshney, D., Rathore, V., Kinger, R., Singh, R.K.: High-pressure induced structural phase transition in alkaline earth  $\text{CaX}$  ( $X = \text{S}, \text{Se}$  and  $\text{Te}$ ) semiconductors: NaCl-type (B1) to CsCl-type (B2). *J. Alloys Compd.* **484**, 239–245 (2009)
29. Varshney, D., Dagaonkar, G., Varshney, M.: Pressure and doping dependent elastic and thermodynamical properties of  $\text{Ga}_{1-x}\text{In}_x\text{P}$  mixed valent compounds. *Mater. Res. Bull.* **45**, 916–926 (2010)
30. Varshney, D., Joshi, G., Varshney, M., Shriya, S.: Pressure induced mechanical properties of boron based pnictides. *Solid State Sci.* **12**, 864–872 (2010)
31. Varshney, D., Kaurav, N., Sharma, U., Singh, R.K.: Pressure induced structural phase transition and elastic behavior of Y and Sc antimonides. *J. Alloys Compds.* **448**, 250–256 (2008)
32. Varshney, Dinesh: Dodiya, N.: Electrical resistivity of the hole doped  $\text{La}_{0.8}\text{Sr}_{0.2}\text{MnO}_3$  manganites: Role of electron–electron/phonon/magnon interactions. *Mater. Chem. Phys.* **129**, 896–904 (2011)
33. Varshney, D., Dodiya, N.: Electrical resistivity of alkali metal doped manganites  $\text{La}_x\text{A}_y\text{Mn}_w\text{O}_3$  ( $A = \text{Na}, \text{K}, \text{Rb}$ ): Role of electron–phonon, electron–electron and electron–magnon interactions. *Curr. Appl. Phys.* **13**, 1188–1198 (2013)
34. Varshney, D., Dodiya, N., Shaikh, M.W.: Structural properties and electrical resistivity of Na-substituted lanthanum manganites:  $\text{La}_{1-x}\text{Na}_x\text{MnO}_3$  ( $x = 0.1, 0.125$  and  $0.15$ ). *J. Alloys Compds.* **509**, 7447–7457 (2011)
35. Shaikh, M., Varshney, D.: Structural properties and electrical resistivity behavior of  $\text{La}_{1-x}\text{K}_x\text{MnO}_3$  ( $x = 0.1, 0.125$  and  $0.15$ ) manganites. *Mater. Chem. Phys.* **134**, 886–898 (2012)
36. Varshney, D., Choudhary, D., Khan, E.: Electrical transport in the ferromagnetic and paramagnetic state of potassium substituted manganites  $\text{La}_{1-x}\text{K}_x\text{MnO}_3$  ( $x = 0.05, 0.1$  and  $0.15$ ). *J. Mater. Sci.* **48**, 5904–5916 (2013)
37. Shaikh, M.W.: Varshney, D.: Structural and electrical properties of  $\text{Pr}_{1-x}\text{Sr}_x\text{MnO}_3$  ( $x = 0.25, 0.3, 0.35$  and  $0.4$ ) manganites. *Mater. Sci. Semicond. Process.* **27**, 418–426 (2014)
38. Millis, A.J.: Cooperative Jahn-Teller effect and electron–phonon coupling in  $\text{La}_{1-x}\text{A}_x\text{MnO}_3$ . *Phys. Rev. B* **53**, 8434–8441 (1996)
39. Millis, J., Littlewood, P.B., Shraiman, B.I.: Double exchange alone does not explain the resistivity of  $\text{La}_{1-x}\text{Sr}_x\text{MnO}_3$ . *Phys. Rev. Lett.* **74**, 5144–5147 (1995)
40. Ederer, C., Lin, C., Millis, A.J.: Structural distortions and model Hamiltonian parameters: From LSDA to a tight-binding description of  $\text{LaMnO}_3$ . *Phys. Rev. B* **76**(155105), 1–11 (2007)
41. Bejar, M., Dhahri, E., Hlil, E.K., Heniti, S.: Influence of A-site cation size-disorder on structural, magnetic and magnetocaloric properties of  $\text{La}_{0.7}\text{Ca}_{0.3-x}\text{K}_x\text{MnO}_3$  compounds. *J. Alloys Compds.* **440**, 36–42 (2007)
42. Radaelli, P.G., Cox, D.E., Marezio, M., Cheong, S.W.: Charge, orbital, and magnetic ordering in  $\text{La}_{0.5}\text{Ca}_{0.5}\text{MnO}_3$ . *Phys. Rev. B* **55**, 3015–3023 (1997)
43. Lide D.R. (Ed.) CRC Handbook of Chemistry and Physics, 79th edn, CRC Press, New York (1999)
44. Buch, J.J.U., Pathak, T.K., Lakhani, V.K., Vasoya, N.H., Modi, K.B.: High temperature thermoelectric power study on calcium substituted lanthanum manganites. *J. Phys. D: Appl. Phys.* **40**, 5306–5312 (2007)
45. Das, S., Dey, T.K.: Structural and magnetocaloric properties of  $\text{La}_{1-x}\text{Na}_x\text{MnO}_3$  compounds prepared by microwave processing. *J. Phys. D: Appl. Phys.* **40**, 1855–1863 (2007)
46. Das, S., Dey, T.K.: Thermoelectric power of potassium doped lanthanum manganites at low temperatures. *J. Magn. Mater.* **311**, 714–723 (2007)
47. Varshney, D., Choudhary, D., Shaikh, M.W.: Electrical resistivity behavior of sodium substituted manganites: electron–phonon,



- Electron–electron and Electron–magnon interactions. *Eur. Phys. J. B* **76**, 327–338 (2010)
48. Varshney, D., Choudhary, D., Shaikh, M.W.: Interpretation of metallic and semiconducting temperature dependent resistivity of  $\text{La}_{1-x}\text{Na}_x\text{MnO}_3$  ( $x = 0.07, 0.13$ ) manganites. *Compd. Mater. Sci.* **47**, 839–847 (2010)
  49. Varshney, D., Choudhary, K.K., Singh, R.K.: Interpretation of temperature-dependent resistivity of electron-doped cuprates. *Supercond. Sci. Technol.* **15**, 1119–1126. (2002)
  50. Wu, D., Deng, Y., Mak, C.L., Wong, K.H., Li, A.D., Zhang, M.S., Min, N.B.: Raman scattering study of La-, Nd and Sm-substituted  $\text{Bi}_4\text{Ti}_3\text{O}_{12}$ . *Appl. Phys. A: Mater. Sci. Process.* **80**, 607–610 (2005)
  51. Jandl, S., Mukhin, A.A., Ivanov, V.Y., Nekvasil, V., Sadowski, M.L.: Raman-active phonons and  $\text{Nd}^{3+}$  crystal-field studies of weakly doped  $\text{Nd}_{1-x}\text{Sr}_x\text{MnO}_3$ . *Phys. Rev. B* **72**(024423), 1–7 (2005)
  52. Marzari, N., Vanderbilt, D.: Maximally localized generalized Wannier functions for composite energy bands. *Phys. Rev. B* **56**, 12847–12865 (1997)
  53. Kubo, K., Ohata, N.: A quantum theory of double exchange. *J. Phys. Soc. Jpn.* **33**, 21–32 (1972)
  54. Ghivelder, L., Castillo, I.A., Alford, N.M., Tomka, G.T., Riedi, P.C., MacManus-Driscoll, J., Akther Hossain, A.K.M., Cohen, L.F.: Specific heat of  $\text{La}_{1-x}\text{Ca}_x\text{MnO}_3$ . *J. Magn. Magn. Mater.* **189**, 274–282 (1998)
  55. Varshney, D., Kaurav, N.: Analysis of low temperature specific heat in the ferromagnetic state of the Ca-doped manganites. *Eur. Phys. J. B* **37** 301–309 (2004)
  56. Varshney, D.: Effect of impurity scatterers on phonon, electron and magnon thermal transport in electron doped cuprate superconductors. *Sup. Sci. Technol.* **19** 433–444 (2006)
  57. Varshney, D., Kaurav, N.: Electrical resistivity in the ferromagnetic metallic state of La-Ca-MnO<sub>3</sub>: Role of electron-phonon interaction. *Eur. Phys. J. B* **40** 129–136 (2004)
  58. Varshney, D., Kaurav, N.: Interpretation of temperature-dependent resistivity of La–Pb–MnO<sub>3</sub>: role of electron–phonon interaction. *J. Low Temp. Phys.* **141** 165–178 (2005)
  59. Varshney, D., Mansuri, I., Kaurav, N.: Effect of electron/hole doping on the transport properties of lanthanum manganites  $\text{LaMnO}_3$ . *J. Phys. Condens. Matter* **19**, 246211 1–13 (2007)
  60. Varshney, D., Shaikh, M. W., Mansuri, I.: Interpretation of temperature-dependent resistivity of  $\text{La}_{0.7}\text{Ba}_{0.3}\text{MnO}_3$  manganites. *J. Alloys Compd.* **486**, 726–732 (2009)
  61. Varshney, Dinesh., Mansuri, I.: Influence of Ce doping on structural and transport properties of  $\text{Ca}_{1-x}\text{Ce}_x\text{MnO}_3$  ( $x = 0.2$ ) manganite. *J. Low Temp. Phys.* **162**, 52–61 (2011)
  62. Mansuri, I., Varshney, D., Kaurav, N., Lu, C.L., Kuo, Y.K.: Effects of A-site disorder on magnetic, electrical and thermal properties of  $\text{La}_{0.5-x}\text{Ln}_x\text{Ca}_{0.5-y}\text{Sr}_y\text{MnO}_3$  manganites. *J. Magn. Magn. Mater.* **323**(2011), 316–323 (2011)
  63. Mansuri, I., Varshney, D.: Structure and electrical resistivity of  $\text{La}_{1-x}\text{Ba}_x\text{MnO}_3$  (0.25 & #x2264; x & #x2264; 0.35) perovskites. *J. Alloys Compd.* **513**, 256–265 (2012)
  64. Varshney, D., Mansuri, I., Kaurav, N., Lung, W.Q., Kuo, Y.K.: Influence of Ce doping on electrical and thermal properties of  $\text{La}_{0.7-x}\text{Ce}_x\text{Ca}_{0.3}\text{MnO}_3$  ( $0.0 \leq x \leq 0.7$ ) manganites. *J. Magn. Magn. Mater.* **324**, 3276–3285 (2012)
  65. Varshney, D., Mansuri, I., Shaikh, M.W., Kuo, Y.K.: Effect of Fe and Co doping on electrical and thermal properties of  $\text{La}_{0.5}\text{Ce}_{0.5}\text{Mn}_{1-x}(\text{Fe,Co})_x\text{O}_3$  manganites. *Mater. Res. Bull.* **48**, 4606–4613 (2013)
  66. Quijada, M., Cerne, J., Simpson, J.R., Drew, H.D., Ahn, K.H., Millis, A.J., Shreekala, R., Ramesh, R., Rajeswari, M., Venkatesan, T.: Optical conductivity of manganites: Crossover from Jahn-Teller small polaron to coherent transport in the ferromagnetic state. *Phys. Rev. B* **58**, 16093–16102 (1998)
  67. Urushibara, A., Moritomo, Y., Arima, T., Asamitsu, A., Kido, G., Tokura, Y.: Insulator-metal transition and giant magnetoresistance in  $\text{La}_{1-x}\text{Sr}_x\text{MnO}_3$ . *Phys. Rev. B* **51**, 14103–14109 (1995)
  68. Malavasi, L., Mozzati, M.C., Azzoni, C.B., Chiodelli, G., Flor, G.: Role of oxygen content on the transport and magnetic properties of  $\text{La}_{1-x}\text{Ca}_x\text{MnO}_{3+\delta}$  manganites. *Solid State Commun.* **123**, 321–326 (2002)
  69. Egilmez, M., Chow, K.H., Jung, J., Fan, I., Mansour, A.I., Salman, Z.: Metal-insulator transition, specific heat, and grain boundary-induced disorder in  $\text{Sm}_{0.55}\text{Sr}_{0.45}\text{MnO}_3$ . *Appl. Phys. Lett.* **92**(132505), 1–3 (2008)
  70. Mannella, N., Yang, W.L., Tanaka, K., Zhou, X.J., Zheng, H., Mitchell, J.F., Zaanen, J., Devereaux, T.P., Nagaosa, N., Hussain, Z., Shen, Z.X.: Polaron coherence condensation as the mechanism for colossal magnetoresistance in layered manganites. *Phys. Rev. B* **76**, 233102 (2007)
  71. Mannella, N., Yang, W.L., Zhou, X.J., Zheng, H., Mitchell, J.F., Zaanen, J., Devereaux, T.P., Nagaosa, N., Hussain, Z., Shen, Z.X.: Nodal quasiparticle in pseudogapped colossal magnetoresistive manganites. *Nature* **438**, 474–478 (2005)
  72. Padmavathi, K., Venkataiah, G., Venugopal Reddy, P.: Electrical behavior of some rare-earth-doped  $\text{Nd}_{0.33}\text{Ln}_{0.34}\text{Sr}_{0.33}\text{MnO}_3$  manganites. *J. Magn. Magn. Mater.* **309**, 237–243 (2007)
  73. Mott, N.F., Davis, E.A.: *Electronic Processes in Non-crystalline Material*, 2nd Edn, Oxford, New York (1979)
  74. Mahendiran, R., Tiwary, S.K., Raychaudhuri, A.K., Ramakrishnan, T.V., Mahesh, R., Rangavittal, N., Rao, C.N.R.: Structure, electron-transport properties, and giant magnetoresistance of hole-doped  $\text{LaMnO}_3$  systems. *Phys. Rev. B* **53**, 3348–3358 (1996)
  75. Das, S., Dey, T.K.: Temperature dependence of the thermoelectric power of  $\text{La}_{1-x}\text{K}_x\text{MnO}_3$  compounds in light of a two phase model. *Phys. B* **381**, 280–288 (2006)
  76. Lakshmi, Y.K., Venkataiah, G., Vithal, M., Reddy, P.V.: Magnetic and electrical behavior of  $\text{La}_{1-x}\text{A}_x\text{MnO}_3$  (A = Li, Na, K and Rb) manganites. *Phys. B* **403**, 3059–3066 (2008)

